Oxidation of UO_2 in dry and wet atmospheres

G. LEINDERS, O. OZDEMIR, J. PAKARINEN, R. DELVILLE and M. VERWERFT
Fuel Materials Group, Nuclear Materials Science Institute, SCK•CEN
Boeretang, 200, B-2400 Mol (Belgium)

ABSTRACT

One of the problems for which currently no quantitative answer can be given, are the degradation kinetics of spent nuclear fuel under different atmospheres. In the present contribution, we report on preliminary results after low-temperature moisturized atmosphere oxidation of UO_2, and the results are compared to recent results of dry air oxidation. The first results indicate that the addition of moisture results in a slight moderation of the oxidation reaction, when compared to dry oxidizing conditions.

1 Introduction

After discharge, spent nuclear fuel is first cooled in deactivation pools at the reactor site until the heat has decayed sufficiently before any further handling can be envisaged. After this decay period, two options are open: reprocessing or interim (dry or wet) storage in preparation of conditioning for geological disposal. In many countries, however, neither of these two options is expected to be implemented within the next decades, leading to the trivial third option: long-term interim storage in which spent fuel is kept in the interim repository for much longer periods than initially foreseen. Ultimately, however, spent fuel assemblies will need to be transported from their interim storage to a facility where they are to be handled in view of final disposal or reprocessing. When embarking on a strategy of long-term intermediate storage, it is mandatory to evaluate how the spent fuel will evolve over these long periods and to quantify effects of non-standard conditions such as defective cladding. In the past, several studies on spent nuclear fuel have been devoted to the effect of moisture on degradation and it appears that when spent fuel is exposed to wet conditions, the UO_2 degradation is more pronounced than for dry air exposure [1,2], but the effect seems to be minor and until today, the debate on the effect of moisture on UO_2 degradation persists [3,4].

Thermodynamically, UO_2 is not stable under ambient conditions: physics dictate that it has a tendency to evolve to the stable chemical form U_3O_8, which involves a volume expansion of ~30% [2]. While thermodynamics predict the tendencies of material evolution, only kinetic models can predict the pace at which such evolution occurs. Today, it is understood that the transformation from UO_2 to U_3O_8 proceeds slowly at low temperatures and that various intermediate phases are formed: UO_{2+x} where $0 \leq x \leq 0.03$ [5], U_4O_{9-y} where $y = 0.0625$ [6,7] (throughout the text the simplified notation U_4O_9 will be used), U_3O_7 [8] and finally U_3O_8 [9]. Until U_3O_7, these intermediate phases induce a net contraction of the bulk but the transformation from U_3O_7 to U_3O_8 is to be avoided. In the entire degradation process, phase transformations from lower to higher oxides compete with oxygen diffusion to the bulk (pumping effect) and one is still far from being able to fully quantitatively assess this process. Of the intermediate phases between UO_2 and U_3O_8, the structure of the last intermediate phase, U_3O_7, has recently been described in a consistent manner by our group [8] and the kinetics of low-temperature, dry atmosphere UO_2 oxidation were also published [10,11].

In the present contribution, we report on preliminary results obtained on low-temperature oxidation of UO_2 powders under a humidified atmosphere. The study enters in the broader research context of spent nuclear fuel degradation and radionuclide release [12], but the results are principally compared to dry atmosphere oxidation, under conditions relevant in the front end of the fuel cycle where the handling of powders is involved.

2 Experimental

2.1 Sample preparation

Sample preparation was done according to a similar process as described in the recent papers on dry air oxidation of UO_2 [10,11,13]. Depleted uranium dioxide was obtained from FBFC International (Dessel, Belgium). The total metallic impurity content was less than 150 µg g^{-1} and was analyzed by inductively coupled plasma mass spectrometry (ICP-MS, ThermoFischer XSeries2); details can be found in [14]. In order to get samples with different specific surface areas (SSA), wet route dissolution and precipitation were used. The as-received powders were first oxidized at 500 °C for 4 hours in an open-atmosphere muffle furnace to get U_3O_8, dissolved in a 6 M HNO_3 aqueous solution, and titrated with an excess of a 6 M NH_4OH aqueous solution. The precipitate formed was washed four times by using pipetting and centrifuging at 1000 rpm for 20 min and dried at 80 °C for several hours in a muffle furnace to obtain ammonium diuranate (ADU) $(NH_4)_2U_2O_7$ powder.

Uranium oxide powders with varying specific surface areas were subsequently prepared from the ADU powder by calcination at different temperatures in the same muffle furnace. At temperatures below 600 °C, UO_3 is expected and at higher temperatures, U_3O_8 forms. After calcination, all samples were analyzed by X-ray diffraction (XRD, PANalytical X'pert Pro diffractometer) to identify their phase composition and by BET analysis (Micromeritics TriStar II 3020) to determine their specific surface. Details can be found in Table 1. In the same table, the preparation details and essential characteristics are given of the powders that were used in already published dry air exposure experiments and to which the current, humid air exposure experiments will be compared. It is interesting to note that slight modifications in the ADU precipitation process may lead to different particle growth during subsequent calcination. After calcination, all powders are α-U_3O_8, except sample M-b, which is still in the β-UO_3 phase, as expected given the lower calcination temperature. Since all further exposure experiments started with in-situ reduction of the powders to UO_2, this difference is not important for the present experiments (see also [10,11]).

Table 1 Sample identification, preparation process parameters and BET analysis. The samples designated by "-a" were prepared earlier for the dry air exposure experiments and the samples designated by "-b" were freshly prepared for humid air exposure. Sample nomenclature is based on the designation used in [10,11]: "M" stands for medium specific surface, "L" for low specific surface.

Sample designation	**L-a**	**M-a**	**L-b**	**M-b**
Calcination conditions	650 °C 4h	650 °C 30 min	650 °C 30 min	500 °C 30 min
SSA (m^2 g^{-1})	4.0	9.3	4.0	11.0
Exposure	Dry	Dry	Humid	Humid

2.2 In-situ oxidation experiments

The oxidation experiments were performed in a Simultaneous Thermogravimetry Analysis instrument (STA), a Netzch STA 449 F1 Jupiter, coupled to a 403 D Aëolos Mass Spectrometer (MS). An oxygen analyzer (Setnag OXYBOX'AIR) and dew point analyzer (Alpha Moisture Systems ADHT-BL) monitored the oxygen and water contents of the exiting gas. A constant flow of argon gas ("protective gas flow", 20 mL min^{-1}) was maintained through the balance compartment and was led into the furnace chamber to improve balance stability. The reactive gas composition varied according to the desired conditions and entered the furnace chamber directly through a second inlet at a flow of 80 mL min^{-1}. The total gas flow was thus 100 mL min^{-1}. The gas supply was controlled via mass flow controllers (Bronkhorst EL-FLOW) which were individually calibrated to the type of gas used.

Powder samples (around 20 mg each) were loaded into a small Pt/Rh crucible with a lid and placed on the sample carrier equipped with a type S thermocouple (Pt-10 % Rh vs. Pt). After loading, the furnace was closed, degassed to 10^{-2} mbar, and refilled with dry argon.
The thermal analysis consisted of three stages. In the first stage, the sample was reduced to stoichiometric UO_2 by heating to 700 °C with an active gas flow of 80 mL min^{-1} of Ar/5 vol% H_2, yielding a combined flow in the furnace chamber of 100 mL min^{-1} of argon 4 vol% H_2. During this stage, the precursor oxide is reduced to UO_2. Then, after cooling to the targeted oxidation temperature T_{ox} (from 40 to 190 °C for the exposure experiments considered here), the furnace chamber was flushed with argon (part 2). In the final isothermal exposure stage (part 3), the samples are isothermally exposed for a period of 14 hours to an active gas flow. The active gas (80 mL min^{-1}) was set to the following conditions:

- synthetic dry air (N_2/21 vol.% O_2) with a very low dew point of -80 °C,
- synthetic humid air, with a dew point of around 17.5 °C,

Humidification was performed on the active gas flow (80 mL min^{-1}) to a dew point of 21.5 °C by setting the controlled evaporation mixer (CEM, Bronkhorst) to an evaporation rate of 0.1 g h^{-1}. In the furnace chamber, the active gas (80 mL min^{-1}) is mixed with dry argon (protective gas flow of 20 mL min^{-1}) and while the actual moisture content (0.1 g h^{-1}) is identical, the dew point of the final gas mixture is thus slightly lower (dew point of 17.5 °C). The STA analyses were corrected for drift and buoyancy by the subtraction of a blank run under identical conditions.

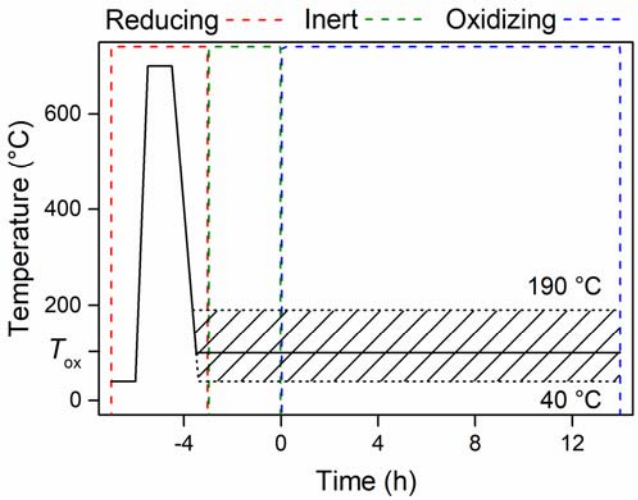

Figure 1 Schematic representation of the in-situ exposures, adapted from [10]. The oxidation temperatures considered here were between 40 °C and 190 °C for all exposure experiments.

2.3 X-ray diffraction analysis

After exposure, the phase composition of the samples were analyzed by Rietveld analysis of X-ray diffractograms acquired on a PANalytical X'pert Pro diffractometer operating in θ–θ configuration, equipped with a LFF Cu X-ray tube (Cu $K_{\alpha 1}$ = 1.5406 Å) and a position-sensitive PANalytical X'Celerator 1D detector with an active length of 2.122°. A Ni filter was used for Kβ elimination, a fixed divergence slit of 0.5° and 0.02 rad Soller slits were applied. Diffractograms were acquired over the range 20° – 120° 2θ. Samples were homogeneously dispersed on a silicon zero background holder with a droplet of isopropanol and left to dry. Rietveld analysis of phase composition was performed with the PANalytical HighScore Plus (v4.6) software according to the procedures set out in the supporting information of [10].

3 Results

3.1 Exposure to dry air

Dry air exposure has been reported earlier [10,11] and in the present paper, we select only the subset of data obtained at temperatures 40 – 190 °C, i.e. at temperatures for which also humid

air exposures were performed. The effect of specific surface area is obvious and expected, and is observed at all temperatures: e.g. at 100 °C after 14 h exposure, a mass increase of respectively 0.9 and 1.9 wt.% occurs in powder with low (4.0 $m^2\ g^{-1}$) and medium (9.3 $m^2\ g^{-1}$) specific surface area [10]. At higher or lower temperatures, the oxidation proceeds to a higher or lower extent, see Table 2 in which the total mass increase is expressed as an elevated average oxygen-to-uranium ratio $(O/U)_{TGA}$). The X-ray diffraction results demonstrate that the oxygen uptake does not lead to a homogeneous solid solution of the form UO_{2+x}, but to the formation of successive higher oxides (see Figure 2). At temperatures below 100 °C, the only phases that form during an exposure of 14 h are slightly hyperstoichiometric $UO_{2.03}$ and U_4O_9, which both exhibit cubic symmetry. At more elevated temperatures the tetragonal U_3O_7 phase starts to develop [10]. The average $(O/U)_{XRD}$ was calculated from the quantitative Rietveld analysis of the XRD data (see Figure 3). At e.g. 100 °C after 14 h exposure, the L-a sample contains roughly 25 wt.% of U_4O_9 ($(O/U)_{XRD}$ = 2.08) while the M-a sample contains already more than 75 wt. % of U_4O_9 ($(O/U)_{XRD}$ = 2.20).

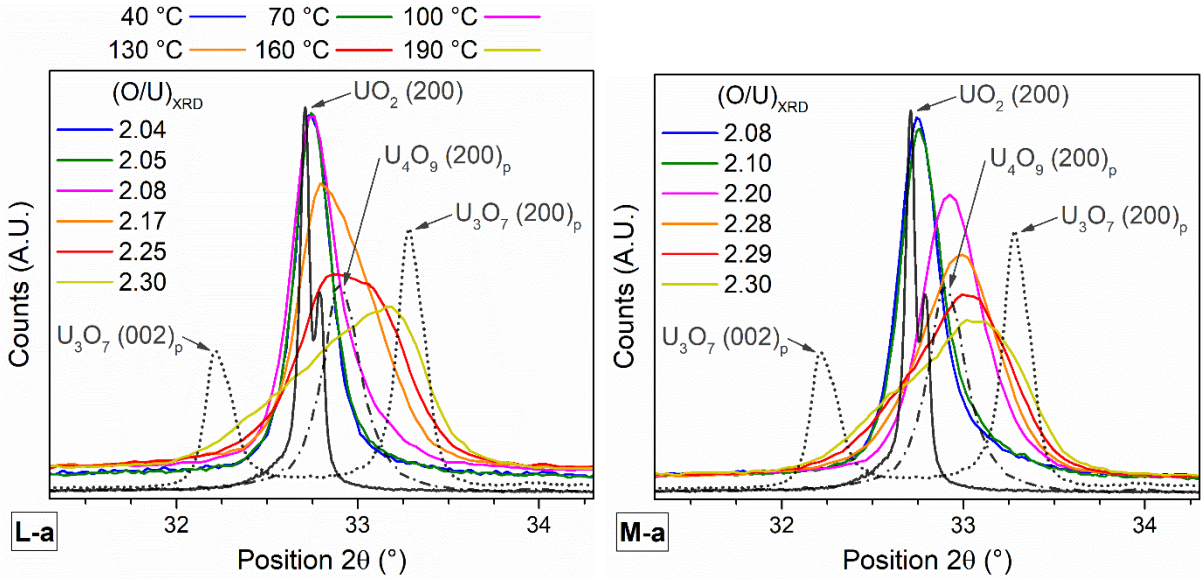

Figure 2 Superposition of X-ray diffractograms (Cu $K\alpha_{1,2}$) near the $(200)_p$ UO_2 reflection of the dry air exposed powders (L-a, M-a), adapted from [10]. Indexation is done according to the parent fluorite structure (hence, subscript "p"). The higher degree of oxidation with increasing temperature results first in a slight peak shift towards higher Bragg angles, due to the fluorite lattice contraction, followed by a more severe shift due to U_4O_9 formation and finally by asymmetric broadening when tetragonal U_3O_7 forms.

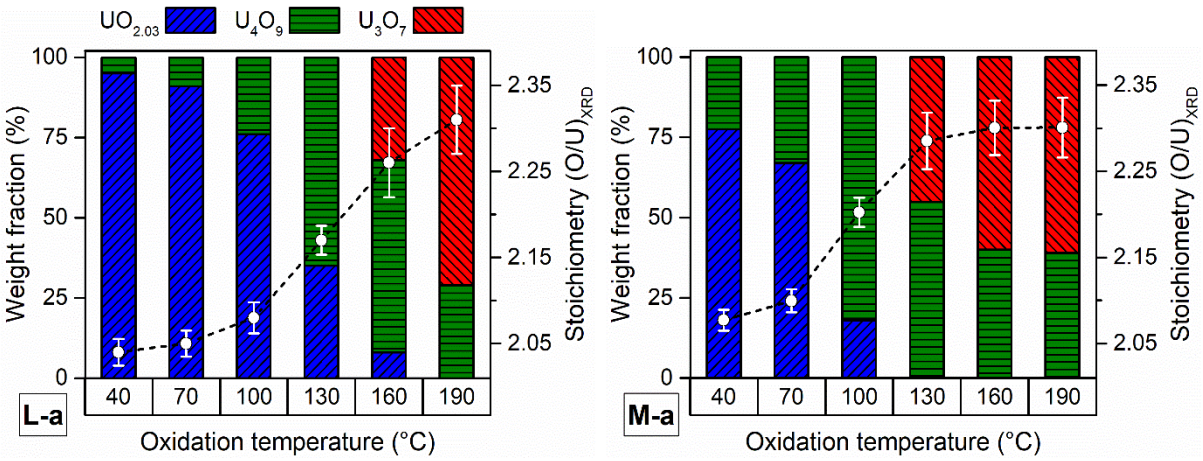

Figure 3 Weight fractions attributed to different crystalline phases in the dry air exposed powders, as determined from Rietveld refinement of the XRD data, adapted from [10]. The refinement is done over the full 2θ range [20°,145°]. The average stoichiometry $(O/U)_{XRD}$ calculated from these results is represented by white dots.

3.2 Exposure to moist air

Similar as for dry air experiments, the effect of specific surface is evident at all oxidation temperatures, resulting in a systematic mass increase. In Table 2 values for $(O/U)_{TGA}$ are reported for ease of comparison with the dry exposure data, however, their interpretation is not as straight-forward: In case the adsorption of moisture on the surface contributes to the total mass increase, the average $(O/U)_{TGA}$ will be overestimated. The effect of temperature was most significant between 100-130 °C for sample L-b, and between 70-100 °C for sample M-b. At more elevated oxidation temperatures up to 190 °C the respective samples reached a limiting $(O/U)_{TGA}$ value of about 2.35 after 14 h exposure. X-ray diffraction data (see Figure 4) demonstrate clearly the formation of U_4O_9 as the extent of oxidation increases, but compared to the dry air exposures, the asymmetric peak broadening which is the signature of U_3O_7 formation is less distinct. Rietveld analysis of the XRD data (see Figure 5) confirmed that at the highest oxidation temperatures both samples contain considerably less of U_3O_7 phase as compared to the dry air exposed samples, i.e. 30-40 wt.% versus 60-70 wt.% respectively.

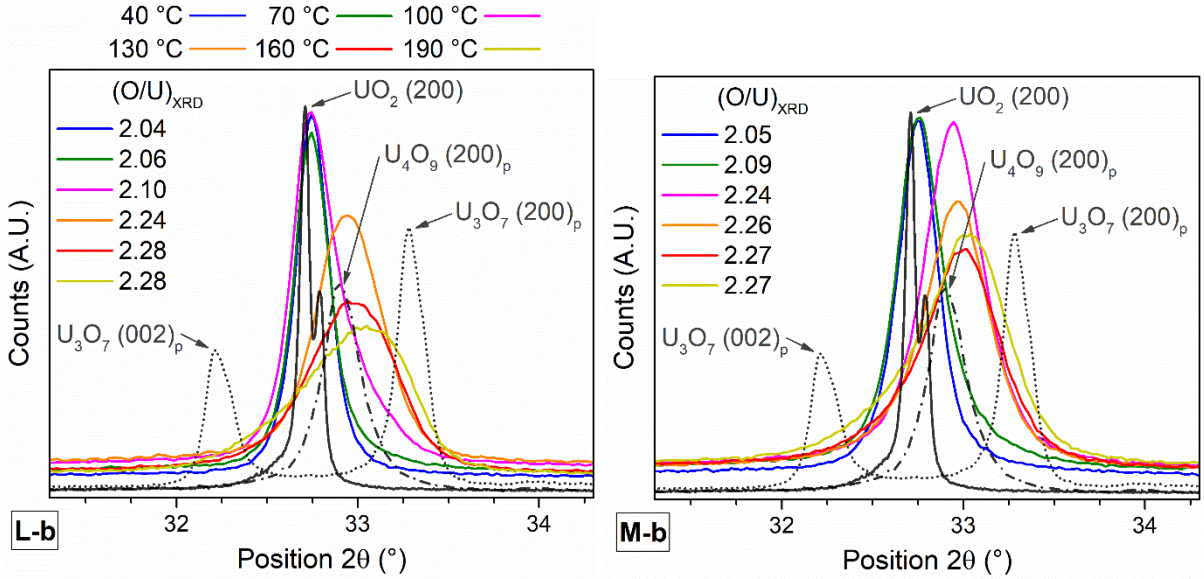

Figure 4 Superposition of the $(200)_p$ reflection (Cu $K\alpha_{1,2}$) in the moist air exposed powders (L-b, M-b). Similar to the dry air exposed powders (Figure 2), oxidation is characterized by first a peak shift towards higher Bragg angles, followed by asymmetric broadening. Compared to the dry air exposures, the asymmetric broadening is less pronounced.

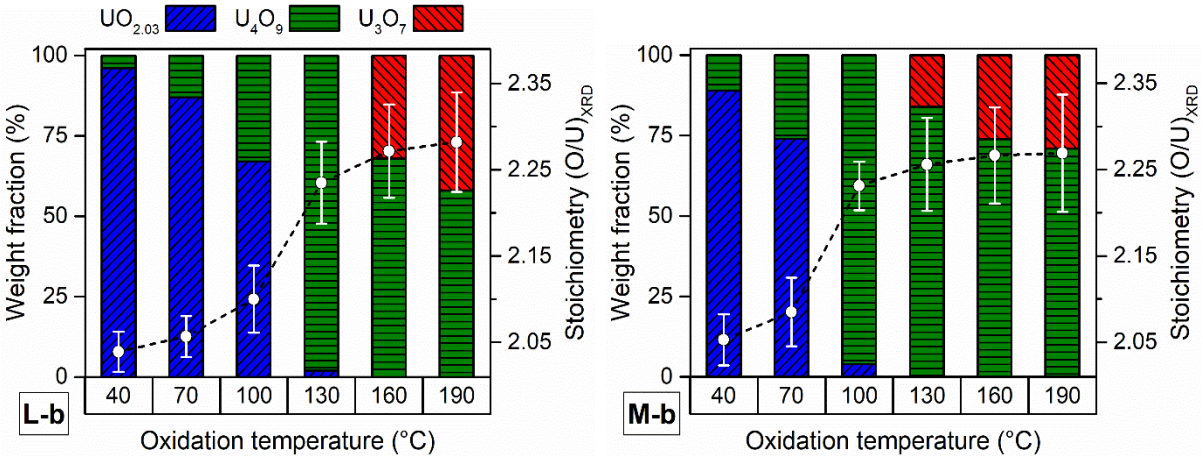

Figure 5 Weight fractions attributed to different crystalline phases in the moist air exposed powders (L-b, M-b), as determined from Rietveld refinement of the XRD data. The refinement is done over the full 2θ range [20°,145°]. The average stoichiometry $(O/U)_{XRD}$ calculated from these results is represented by white dots.

Table 2 Experimental results of dry [10] and moisturized air exposure of UO_2 powders at temperatures between 40 °C and 190 °C, after 14 h exposure time. The $(O/U)_{TGA}$ values were calculated from TGA measurements, and can be slightly overestimated when adsorption reactions on the surface are involved. The $(O/U)_{XRD}$ values were derived from phase analysis of the XRD data, but do not take into account the possible contribution of amorphous phases.

	$(O/U)_{TGA}$				$(O/U)_{XRD}$			
	Dry		Wet		Dry		Wet	
Temperature (°C)	**L-a ±0.02**	**M-a ±0.02**	**L-b ±0.03**	**M-b ±0.03**	**L-a ±0.02**	**M-a ±0.02**	**L-b ±0.03**	**M-b ±0.03**
40	2.06	2.13	2.04	2.07	2.04	2.08	2.04	2.05
70	2.08	2.19	2.07	2.11	2.05	2.10	2.06	2.09
100	2.15	2.32	2.19	2.29	2.08	2.20	2.10	2.23
130	2.26	2.39	2.34	2.35	2.17	2.28	2.24	2.26
160	2.33	2.39	2.34	2.36	2.25	2.29	2.27	2.27
190	2.38	2.42	2.35	2.35	2.30	2.30	2.28	2.27

4 Discussion

The setup for dry atmosphere exposure has recently been extended with a capability to expose samples to an atmosphere with controlled moisture content and in the present study, the first results of UO_2 powder oxidation under moist atmospheres are reported. Compared to studies on solid material, which are conducted on e.g. polished cross sections of sintered pellets or single crystals, the reactive surface is much larger for powders (e.g. a 20 mg sample of a powder with SSA 10 m^2 g^{-1} has a reactive surface of 0.2 m^2 or 2 000 cm^2) and represents a difference of several orders of magnitude. In a recent study fragments of UO_2 pellets were exposed to dry and moisturized air at temperatures up to 100 °C for an extended period of 39 days, but no clear influence of humidity was observed [15]. Working with powders of different SSA furthermore allows one to investigate if the specific exposure setup is impacting the results. This might e.g. be the case when the flow of oxidizing species is too low and hence becomes rate-limiting for the corrosion reaction. Proper conditions are achieved when the instrumental setup is not impacting the result obtained from a series of samples with different SSA, but otherwise identical [11].

A systematic mass increase as a function of oxidation temperature occurs in all samples (see Table 2). In case of the moisturized air exposures the $(O/U)_{TGA}$ values measured for the M-b sample are consistently below the respective values of the M-a sample. Similarly, the degree of oxidation observed in the XRD data was always lower, except for an outlier at 100 °C exposure temperature (but still within the reported uncertainty). Taking further into account that sample M-b has actually a 20% higher initial specific surface than sample M-a (11.0 versus 9.3 m^2 g^{-1}, respectively), this shows that the effect of moisture is counter-intuitive: no evidence for an enhanced corrosion was observed.

The data of sample L-b show no significant difference in terms of mass increase and degree of oxidation as compared to sample L-a, considering reported uncertainties. Only at an exposure temperature of 130 °C oxidation proceeded to a considerably higher extent in sample L-b. The reproducibility of these results will be further investigated, but the insignificant difference between both exposure conditions on low surface area samples, does agree with recent reports on UO_2 pellet fragments [15].

It remains to be investigated whether all mass increase can be attributed to a process of corrosion. It is possible that the formation of amorphous UO_3 or UO_3 hydrate, which are in the considered temperature domain both thermodynamically more stable than the other oxides of UO_2, including U_3O_8 [16,17], is involved. Amorphous nano-domains were also observed in recent oxidation experiments [10]. In addition, the adsorption of water and/or oxygen molecules on the surface of the UO_2 grains may also influence the kinetics of the oxidation reaction.

5 Conclusions

Uranium dioxide powders with different specific surface area were exposed to dry [10,11] and humidified oxidizing atmospheres in the temperature range 40 – 190 °C. The presence of moisture did not enhance the corrosion reaction in the medium surface area samples, but instead, the results show a very slight moderation of the reaction as compared to the dry oxidizing conditions. Whether adsorption reactions or formation of amorphous phases on the surface play a role remains to be further investigated.

6 References

[1] A. Leenaers, L. Sannen, S. Van den Berghe, M. Verwerft, J. Nucl. Mater., 317 (2003) 226.
[2] R.J. McEachern, P. Taylor, J. Nucl. Mater., 254 (1998) 87.
[3] C.L. Tracy, C.H. Chen, S. Park, M.L. Davisson, R.C. Ewing, J. Nucl. Mater., 502 (2018) 68.
[4] S.B. Donald, M.L. Davisson, Z.R. Dai, S.K. Roberts, A.J. Nelson, J. Nucl. Mater., 496 (2017) 353.
[5] R.J. McEachern, P. Taylor, J. Nucl. Mater., 254 (1998) 87.
[6] C. Rocanière, J.P. Laval, P. Dehaudt, B. Gaudreau, A. Chotard, E. Suard, J. Solid State Chem., 177 (2004) 1758.
[7] D.J.M. Bevan, I.E. Grey, B.T.M. Willis, J. Solid State Chem., 61 (1986) 1.
[8] G. Leinders, R. Delville, J. Pakarinen, T. Cardinaels, K. Binnemans, M. Verwerft, Inorg. Chem., 55 (2016) 9923.
[9] B.O. Loopstra, Acts Cryst., 17 (1964) 651.
[10] G. Leinders, J. Pakarinen, R. Delville, T. Cardinaels, K. Binnemans, M. Verwerft, Inorg. Chem., 55 (2016) 3915.
[11] G. Leinders, T. Cardinaels, K. Binnemans, M. Verwerft, Inorg. Chem., 57 (2018) 4196.
[12] "Spent Fuel Autoclave Leaching (SF-ALE) project for the release of radionuclides from spent nuclear fuel under representative conditions of water chemistry and oxygen activity Partners: NIRAS/ONDRAF, FZ-Jülich, SCK•CEN", in, 2017.
[13] G. Leinders, R. Bes, J. Pakarinen, K. Kvashnina, M. Verwerft, Inorg. Chem., 56 (2017) 6784.
[14] G. Leinders, T. Cardinaels, K. Binnemans, M. Verwerft, J. Nucl. Mater., 459 (2015) 135.
[15] C.L. Tracy, C.-H. Chen, S. Park, M.L. Davisson, R.C. Ewing, J. Nucl. Mater., 502 (2018) 68.
[16] H.R. Hoekstra, S. Siegel, J. Inorg. Nucl. Chem., 18 (1961) 154.
[17] P. Taylor, R.J. Lemire, D.D. Wood, Nucl. Technol., 104 (1993) 164.